14

The Advantages of Polymer Composites with Detonation Nanodiamond Particles for Medical Applications

L. Pramatarova et al*
Georgi Nadjakov Institute of Solid State Physics,
Bulgarian Academy of Sciences, Sofia
Bulgaria

1. Introduction

An important goal of materials science is the development of interfaces that integrate the functions of living cells and materials. Nature has given us plenty of ideas on how to build composites and organized structure (Heuer et al. 1992, Lowenstam, Weiner, 1989). The structure of a given biomaterial is crucial, when determining the cell response, and respectively the variants for its biomedical applications. The combined unique properties offered by organic and inorganic constituents within a single material on a nanoscale level make the nanocomposites attractive for the next generation of biocompatible materials. In this case, the composite materials of the type detonation nanodiamonds/polymers possessed spatial organization of components with new structural features and physical properties, as well as complex functions due to the strong synergistic effects between the nanoparticles and polymers. Recently, there is a growing interest in the synthesis of composite functional materials with new physico-chemical properties, involving integration of inorganic nanomaterials into a polymer matrix (Shenderova et al., 2002, Dolmatov, 2007, Borjanovic, 2000). Numerous siloxan-based materials, including polymerized hexamethyldisiloxane (PPHMDS) are developed. PPHMDS was easy to prepare by a well established technology of plasma polymerization (Vasilev et al., 2010, Radeva et al., 1993). PPHMDS has a long history of exploitation in a variety of applications, because it is non-toxic, transparent, with a very low surface tension, flexible, and it neither dissolves nor swells in a cell culture medium (Min-Hsien, 2009). On the

*E. Radeva[1], E. Pecheva[1], T. Hikov[1], N. Krasteva[2], R. Dimitrova[3], D. Mitev[4], P. Montgomery[5], R. Sammons[6] and G. Altankov[7,8]
1 Georgi Nadjakov Institute of Solid State Physics, Bulgarian Academy of Sciences, Sofia, Bulgaria
2 Institute of Biophysics, Bulgarian Academy of Sciences, Sofia, Bulgaria
3 Institute of Organic Chemistry, Bulgarian Academy of Sciences, Sofia, Bulgaria
4 Space Research Institute, Bulgarian Academy of Sciences, Sofia, Bulgaria
5 Institut d'Electronique du Solide et des Systemes, UDS-CNRS, Strasbourg, France
6 School of Dentistry, University of Birmingham, Birmingham B4 6NN, UK
7 Institut de Bioenginyeria de Catalunya, Barcelona, Spain
8 ICREA (Institució Catalana de Recerca i Estudis Avançats), Catalonia, Spain

other hand, nanodiamond structures are of interest due to combination of unique properties inherent to diamond and the specific surface structure of particles facilitating its fictionalization (Shenderova et al., 2002). The detonation nanodiamonds (DND), synthesized by detonation of carbon-containing explosives, are produced with particles mostly 4 nm and could be easily modified by appropriate chemical reactions. The Si-DND samples, obtained by silinaztion are produced in order to prevent formation of DNDs aggregates (Baidakova, Vul', 2007). The incorporation of silver ions in the polymer, lead to production of samples that are highly efficient against bacterial colonization and allows the adhesion and spreading of mammalian cells (Vasilev K et al., 2010, Agarwal et al., 2009). It is found that the adhesion and proliferation of different types of cells on biomaterials depend on many surface characteristics, such as surface charge, wettability (hydrophobicity/hydrophilicity), chemistry, microstructure, roughness, and mechanical properties (Min-Hsien, 2009). For cell culture processes, fibronectin (FN) treatment is one of commonly used approaches to enhance the cell adhesion on a surface (Salmerón-Sánchez, Altankov, 2010). In our biological experiments, the role of FN for the cellular interaction with the plasma obtained structures was also estimated regarding potential biomedical implication.

In the presented paper, we assume that the osteoblast cell behavior could be modulated by substrates surface properties that might be extremely important for the potential osseointegration of such materials. For that reason, the development of technology for production of DND-based polymer composites by plasma polymerization (DNDs/PPHMDS) of a mixture of hexamethyldisiloxane (HMDS) monomer and DNDs on different solid substrate is discussed and the resultant composites are characterized by SEM, AFM, FTIR, Raman, Contact angle and XPS techniques. We pay particular attention on composite surface topology and chemical nature, as the use of DND can be regarded as a collagen analog and can secure the architectural plan for mineralization of hydroxyapatite (Zhao et al., 2005, Pramatarova et al., 2007). We also examine the effect of ammonia plasma treatment of the composites as such modification is an easy way to render the hydrophobic surface into hydrophilic and thus to develop substrates that support the initial interaction of adherent cells.

2. Experimental

2.1 Deposition of PPHMDS

Poly(hexadimethylsiloxan) layers were prepared by plasma polymerization technology as previously described (Radeva et al., 1993). The monomer hexamethyl disiloxan (HMDS) was purchased from Merck, Germany [$(CH_3)_3$-Si-O-Si-$(CH_3)_3$] with a purity of 99.99% and used without further purification. Information about the plasma reactor and the process is given elsewhere (Tsankov et al., 2005, Radeva, Spassov, 1998). Briefly, the plasma excitation of the HMDS gas was achieved at 27. 12 MHz and the current density was 0.04 mA/cm^2. The HMDS flow rate and ammonia (NH_3) vapors were carried out by special inlet micro-valves (GMR, NOVIS, Bulgaria). The substrates were placed on a Teflon plate (190 mm in diameter) half way between the two electrodes. The PPHMDS deposition was carried out in air, at vacuum higher than 100 Pa and for a period from 5 to 40 min. The PPHMDS and composites (DNDs/PPHMDS) were deposited on cover glass (CG) slips (12 mm in diameter), on stainless steel AISI 316 (SS) (8 x 8 x 1 mm in size), on pieces of (Wacker) silicon (Si) wafer, on

KBr as well as on the surface of the quartz resonator), used as quartz microbalance (QCM). Before the deposition, the substrates were chemically and plasma cleaned (Radeva et al., 1993).

2.2 NH_3 plasma treatment of PPHMDS and DNDs/PPHMDS

The treatment of PPHMDS and DNDs/PPHMDS by NH_3 plasma was carried out in the same reactor at 0.04 mA/cm^2 current density and 10 l/h monomer flow rate, varying the time of the treatment from 30 sec to 10 min.

2.3 DND nanoparticles and their surface modification

The DNDs were used in a form of powder and suspension. The powders (6-DND and modified Ag-DND and Si-DND) were synthesized by the Space Research Institute, Bulgarian Academy of Sciences, Sofia, Bulgaria (Stavrev et al., 1994).

6-DND powder: The initial nanodiamonds synthesis was carried out by use of carbon-containing explosive mixtures – conical cast charges (0.6 kg) consisting of TNT/RDX in ratio 70/30. The blasting of the charges was made in a spherical explosion camera with inner volume of 3 m^3, in presence of water as cooling media (wet synthesis). The purification of the diamond powder was done as follows: boiling in a solution of stoichiometrically calculated amounts of potassium dichromate ($K_2Cr_2O_7$) in sulfuric acid (H_2SO_4) at 100-115^{o}C, followed by several water washings and additional removing of metal impurities by HCl-treatment (80-100^{o}C) and washing with water until pH=7. The prepared DND powder was characterized by FTIR-spectroscopy, oxidative titration, and pH-measurement as described in (Mitev et al., 2007). The high-magnification TEM micrograph indicates that the studied material consists of diamond nanoparticles whose sizes are below 10 nm. The small amount of silicon present (less than 1%) makes it difficult to locate.

Ag-DND powder: The ammonia complex of silver ($[Ag(NH_3)_2]^+$) was added to 6-DND-suspension under constant stirring at room temperature followed by adding of a dextrose solution. The temperature of the mixture was raised to 50^{o}C until the Ag incorporation into the DND surface was finalized.

Si-DND powder: The silanization of 6-DND surface through an attachment of trimethylsilyl groups was done by mixing of a dehydrated 6-DND with ethyl acetate containing hexamethyldisilazane and trimethylchlorosilane. After the reaction, the excess of the reagents was removed by microwave heating of the sample in butyl acetate medium. The side-produced ammonium chloride and the excess of butyl acetate were removed through threefold treatment/decanting with methanol. Si-DND sample was finally microwave dried.

7-DND suspension: This nanodiamond was synthesized by Ukrainian company Alit, Kiev. The production method is similar to the described above wet synthesis, but larger charges (up to tens of kilograms) and larger explosion camera (100 m^3) were used. The purification of diamond powder from the attending admixtures was done using stoichiometric mixture of H_2SO_4 and chromium anhydride. After purification, the diamond powder was dipersed in ethanol (C_2H_5OH) by ultrasonic treatment and intensive stirring in presence of milling particles (larger diamond monocrystals. The concentration of DND in the suspension is 0.7 % with average particle size - 50 nm. (Bogatyreva et al., 2008)

2.4 Deposition of DNDs/PPHMDS composites

The composites deposition was carried out in the same plasma polymerization equipment as described in section 2.1. The following procedure was applied: DND powder was added to HMDS monomer in a range of 0.01 – 0.10 g/100 ml and shaked for 15 min in an ultrasonic apparatus; further the container with the mixture was stirred (275 r.p.m) continuously at room temperature. The process of plasma polymerization was performed at about 0.09 mA/cm^2 current density and 10 l/h flow rate for 40 minutes. The subsequent modification by ammonia plasma for 5 min was described in section 2.2.

2.5 Characterization of PPHMDS and DNDs/PPHMDS

2.5.1 Scanning electron microscopy (SEM)

The surface topography of PPHMDS and DNDs/PPHMDS composites, grown on Si substrate were examined by SEM (Carl Zeiss NTS GmbH apparatus), applying original experience (Low Loss BSE Imaging with ZEISS ULTRA GEMINI technology). The thickness of the layers was calculated from the observed cross sections.

2.5.2 Atomic force microscopy (AFM)

AFM was performed using an SMENA AFM, NT-MDT, Russia, software NOVA RC1 with silicon cantilever. The images were recorded in tapping mode under ambient conditions and are with size of 100 nm – 50 μm, lateral resolution 10 nm, vertical resolution 1 nm, layer height possible of max 1 μm and a scanning area of 20 × 20 μm. The root mean square (RMS) roughness of the film was measured.

2.5.3 Fourier Transform Infrared Spectroscopy (FTIR)

FTIR spectra of the of PPHMDS and DNDs/PPHMDS composites were registered by Brucker FTIR spectrometer at ambient temperature in the range of 400 to 4000 cm^{-1} , using OPUS software, average of 64 scans and a resolution of 2 cm^{-1}. The assignment of the absorption bands was based on experience with organic compounds and the literature data. The quoted wavelengths are believed to be within 2 or 3 cm^{-1} of the true values.

2.5.4 Raman spectroscopy

Room temperature resonance Raman spectra of PPHMDS and DNDs/PPHMDS structures, grown on Si substrate were measured using a micro Raman spectrometer (Jobin-Ivon, HR 800) with a grating 600 gr/mm.

2.5.5 Contact angle measurements (CA)

Samples water contact angles were measured through the sessile drop shape method under ambient conditions. Static water contact angle was measured on a Krüss contact-angle system (DSA10, Krüss GmbH, Germany) on freshly prepared surfaces. A 20 ± 2 μL deionized water was dropped onto the investigated surface and the water drop was photographed. The shape of the drop was then analysed using a sessile drop fitting model. Contact angles on five different regions on each sample were measured and averaged.

2.5.6 X-ray Photoelectron spectroscopy (XPS)

XPS analysis was applied to determine the composition and chemical states of the main elements present in the samples. XPS analyses have been performed on VG ESCALAB Mk II

Scientific spectrophotometer; with Al Kα (1486.6 eV) exciting radiation; take off angle - 90°; energy resolution – 1.0 eV.

2.5.7 Dynamic light scattering (DLS)

Particle size distribution of DNDs in HMDS monomer was measured at 20°C in back scatter geometry using a Malvern Zetasizer Nano ZS (Malvern Instruments Ltd, UK) equipped with a 10 mW HeNe laser (633 nm).

2.6 Biocompatibility studies

2.6.1 *In vitro* cytotoxicity test

To study cytotoxicity of DND nanoparticles an established monolayer of cells was exposed to suspensions or supernatants of DND for 72 hours. At the end of the treatment cell viability was monitored by FDA - a fluorescent assay based on the ability of living cells to hydrolyze nonfluorescent compound fluorescein di-O-acetate (FDA) to fluorescein. A human osteosarcoma MG63 cell line (ATCC, USA) was used in these studies, and further, for cell adhesion experiments. Cell monolayer was formed after seeding the cells onto glass coverslips at a concentration of $5x10^4$ cells/ml and 24 h-incubation in serum-containing medium. Then the DND suspensions or supernatants were added to the medium. Suspensions were prepared by adding DND powder in DI water at a concentration 100 µg/ml. Before adding to the cells, the suspensions were washed three times in culture medium then 50 µl from each sample was added to the cells. Extracts were prepared by incubation of DND nanoparticles in cell culture medium (DMEM) for 24 h at 37^0. Then 100 µl supernatants was added to the cell monolayer. After 72 h cell viability was determined as follows: the medium was gently aspirated, the cultures rinsed once in phosphate-buffered saline (PBS, pH 7.4) and stained with 5 ul 0,001% FDA (Sigma, Germany) in acetone. After 2 min the cells were rinsed with PBS to remove unbound stain and examined by inverted fluorescence microscope (Zeiss, Axiovert) and digitally photographed.

2.6.2 Adhesion assays

MG63 osteoblast-like cells were seeded on composite films (DNDs/PPHMDS) individually placed in 24-well tissue culture plates (Costar, USA) at a density of 50000 cells/well. Before cell seeding half of the samples were pre-adsorbed with fibronectin (Roche, Germany, 20 µg/ml in PBS) for 30 min at RT. The cells were incubate for 2 hours in serum-free culture medium (DMEM, Sigma) before to be fixed, permeabilized and stained for actin and vinculin in order to visualize the overall cell morphology (at low mag) and the development actin cytoskeleton and focal adhesion contacts as previously described (Krasteva et al., 2010).

3. Results

The results are presented as follows. Primary, FTIR and contact angle (CA) characterization of plasma obtained polymer (PPHMDS) and its surface modification by ammonia plasma treatment are reported. The aim was to disclose the properties of PPHMDS surface and its modification after interaction with NH_3 molecules. Next, characterization of DND/PPHMDS composites is provided, which comprise a characterization of the DND nanoparticles (TEM,FTIR and UV spectroscopies) as well as particle size distribution (PSD)

of DND in HMDS monomer. Data for DNDs/PPHMDS composites by SEM, AFM, CA, FTIR and Raman, Ellipsometry and XPS are shown. Finally, the Bacteria and Cell experiments are presented in order to evaluate the suitability of the obtained composites for biological application.

3.1 Characterization of PPHMDS

3.1.1 FTIR of PPHMDS and PPHMDS treated by ammonia plasma

The FTIR spectrum of PPHMDS and the spectra of the samples treated by NH_3 plasma are presented in Fig. 1. The formation of PPHMDS layer on CG (Fig. 1-1) is well proved from the characteristics peaks at around 1000 cm^{-1} and 1500 cm^{-1} and above 3500 cm^{-1}.

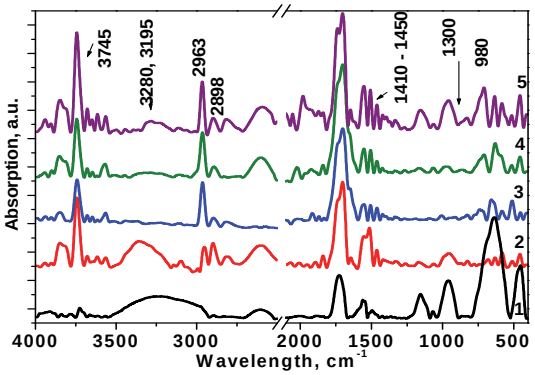

Fig. 1. FTIR spectra of (1) PPHMDS; (2) PPHMDS treated by NH_3 plasma for 30sec; (3) for 1 min; (4) for 5 min and (5) for 10 min.

The asymmetric stretching vibration of the Si–O–Si at around 1165 cm^{-1} evidences for a formation of cross linked Si-O-Si network which is well-defined on CG, since the triple peaks are observed in the region. The strong unresolved peak at 700 cm^{-1} pointed to the existence of various different tetrahedral arrangement of CH_3 groups connected to silicon atoms, while the stretching mode from the C–H bond in the Si–CH_3 group is with a maximum at 460 cm^{-1}. Groups in the region 1500-1700 cm^{-1} pointed to carbonyl functionalities incorporated into the polymer and the presence of OH groups. It is worth to note that referent polymer spectra on the KBr revealed differences that is a verification for the chemical interaction between the substrate (CG) and the plasma formed layer (Radeva et al., 2010). The FTIR spectra of PPHMDS treated by NH_3 plasma are significantly changed as shown in Fig 1- (2-5). The FTIR spectra of PPHMDS treated by NH_3 plasma are significantly changed as shown in Fig 1- (2-5) and in the deconvolution spectra in the characteristic range from 1200 – 800 cm^{-1} (Fig. 2 a, b).

The results from backscattered high energy ion beam (RBS) (not presented) confirmed this suggestion. Based on these studies we concluded that the grown PPHMDS layers are with excellent adhesion to the substrates and their surface could be significantly modified by the grafted ammonia molecules in order to become with hydrophilic nature (www.ism.kiev.ua).

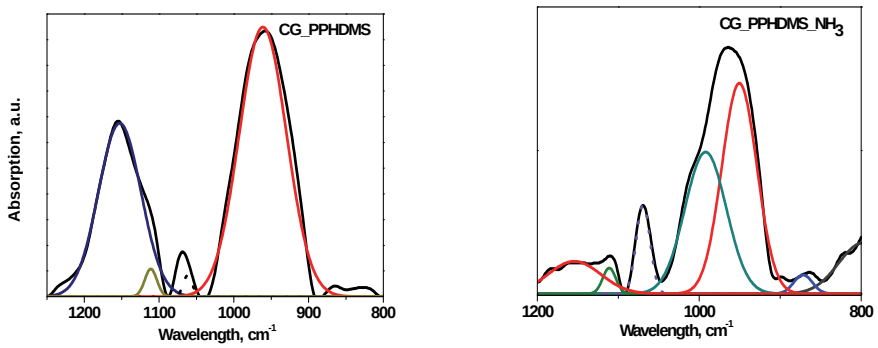

(a) (b)

Fig. 2. Deconvolution spectra in characteristic FTIR range from 1200 – 800 cm^{-1} for the PPHMDS chain (a) and PPHMDS treated with NH_3 plasma (b).

3.1.2 Contact angle of PPHMDS and PPHMDS treated by NH_3 plasma

The water contact angle (CA) of PPHMDS layer, with a thickness of about 300 nm was measured to be $90^0 \pm 2^0$. In our previous works it was found that the CA for thinner PPHMDS layers (60-100 nm) was about $83^0 \pm 2^0$ (Krasteva et al., 2010a, 2010b). The PPHMDS layer thickness is related to its optical properties as found by the Ellipsometry measurements (not presented). So, we suppose that the CA could provide information about PPHMDS layer surface energy, and correspondingly about PPHMDS surface wettability and the hydrophobisity (Pihan et al., 2009, Radeva et al., 2010). The data presented in (Table 2, section 3.3.3.) illustrate the CA change after 5 min layers treatment by NH_3 plasma. The CA of the thick layers diminished from $90^0 \pm 2^0$ to $85^0 \pm 2^0$. For the thin layers, the applied 5 min NH_3 plasma treatment is sufficient for obtaining hydrophilic polymer surface as the measured CA is about 40^0 – 35^0 (Krasteva et al., 2010a, 2010b).

3.2 Characterization of DNDs used as filler in PPHMDS

3.2.1 TEM of DND

The HRTEM images of the 6-DND, Si-DND and Ag-DND are shown in Figure 3 and 4.

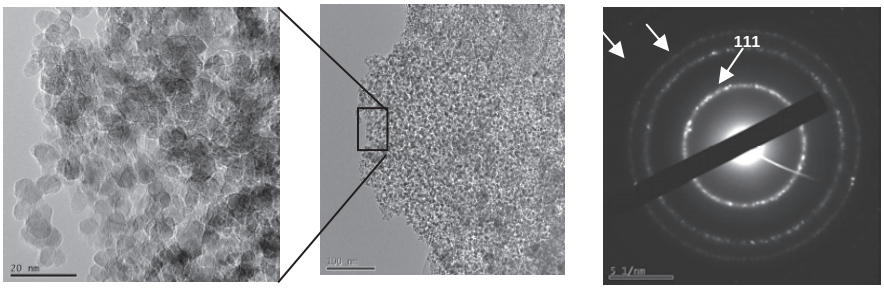

Fig. 3. HRTEM images and diffractogram of Si-DND powder. Scale bars correspond to 100 nm (right image) and to 20 nm (left image).

No specific structure is seen for Si-DND. The selected area of 1 μm shows that Si-DND is with better crystallinity than 6-DND and Ag-DND. The diffraction pattern corresponding to the (111) crystallographic plane of the diamond is observed by the bright contrast line. In Fig. 4, particles agglomerations with nano-grains are observed. The diffraction pattern of Ag-DND corresponds to the diamond one. No additional spot or ring, corresponding to metallic silver is observed. The diffraction rings are thin and punctuated by bright dots that indicate larger than 6 nm Ag-DND nanoparticles.

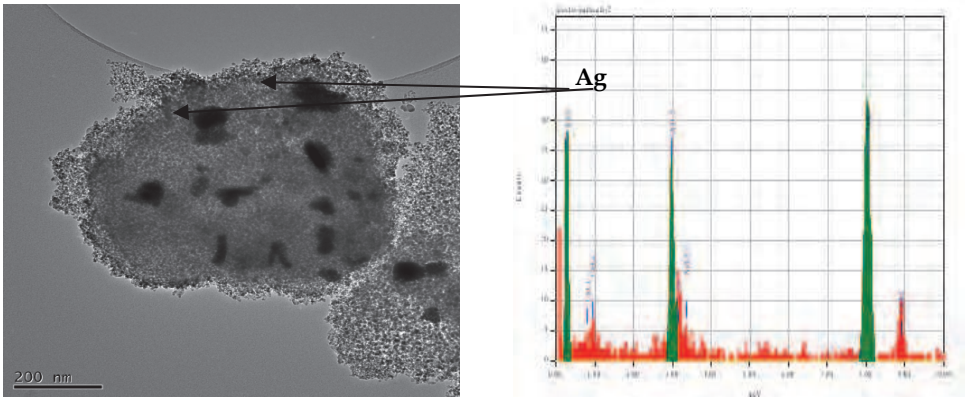

Fig. 4. HRTEM image and EDX of Ag-DND. The scale bar corresponds to 200 nm.

3.2.2 FTIR and UV spectroscopy of DND

The FTIR and UV-visible absorption spectra of DNDs are presented in the Fig. 5 and Fig. 6. The spectra provide evidence that all materials possessed hydrophilic surface that is chemically multifunctional. In the FTIR spectrum of 6-DND, the broad peak at 400±700 cm^{-1} evidence for amorphous sp^3 bonded carbon, while the relatively sharp peaks at 1000 - 1150 cm^{-1} show the presence of sp^2 bonded carbon atoms. The absorption peaks in the range 1500 - 1800 cm^{-1} are ascribed to C=O stretches of different nature. The aliphatic C-H stretching vibrations are well resolved in the range from 2870 cm^{-1} to 2980 cm^{-1} and the presence of hydroxyl species is revealed by the strong band at 3440 cm^{-1} (Fig 5–1).

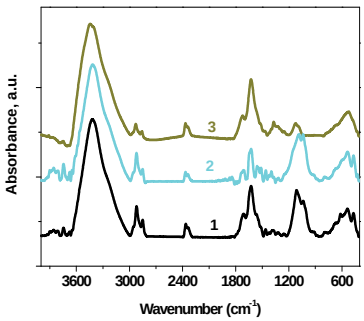

Fig. 5. The FTIR spectra of the DNDs powders used as a filler of PPHMDS: (1) 6- DND; (2) Si-DND; (3) Ag-DND;

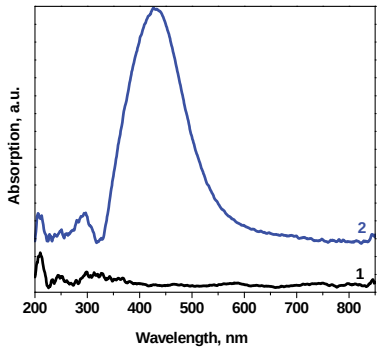

Fig. 6. UV-visible absorption spectra of the synthesized DNDs: (1) 6-DND; (2) Ag-DND;

The incorporation of Ag cations on DND surface (Fig 5–3), is established by the diminishing of the FTIR peaks in the region about 1100 cm^{-1}, the appearance of new peaks at around 1300 cm^{-1}. The silanization of DND surface (Fig 5-2), is revealed through the increase of the sp^2 bonded carbon atoms (peaks at 1000 - 1150 cm^{-1}) and the diminishing of the acidic surface functional groups observed in the region 1500 – 1750 cm^{-1} due to formation of new Si-O-C bonds.

The low intensive peaks at about 210 and 280 nm have point to formation of the Ag_2^+ and small silver clusters (Ag_n) (Fig.6). The appearance of a plasmon peak higher than 410 nm indicated the formation of Ag nanostructures (Hong et al., 2006, Murphy, Jana, 2002).

3.2.3 Particle size distribution of DNDs in HMDS monomer

The monomer mixture with DNDs powders was prepared according the protocol, described in the experimental part. The corresponding suspensions of 6-DND, Si-DND, Ag-DND and the monomer (HMDS) in a relation 0.01g/100ml were sonificated for 10 min and then diluted with pure HMDS in a ratio 1:10. The data for the mean size of the DNDs particles measured by peaks intensities are presented in Table 1.

Sample Name	Z-Ave (d.nm)	Poly Dispertion	Pk 1 Mean Int (d.nm)	Pk 2 Mean Int (d.nm)	Scattering Angle (°)	Diffusion Coefficient (μ?/s)
Ag-DND/HMDS	1083	0,814	196,1	3,697	173	0,448
Si-DND/HMDS	302,7	0,31	189,6	0	173	1,6
6-DND/HMDS	2236	1	215,3	0	173	0,217

Table 1. Particle size distribution of DNDs, given by intensity (Nobbmann, Morfesis, 2009).

3.3 Characterization of DNDs/PPHMDS composites

3.3.1 SEM of DNDs/PPHMDS composites

In order to obtain SEM image from our low-dense materials we apply new experience to visualize the weak signals (Heiner, 2008).

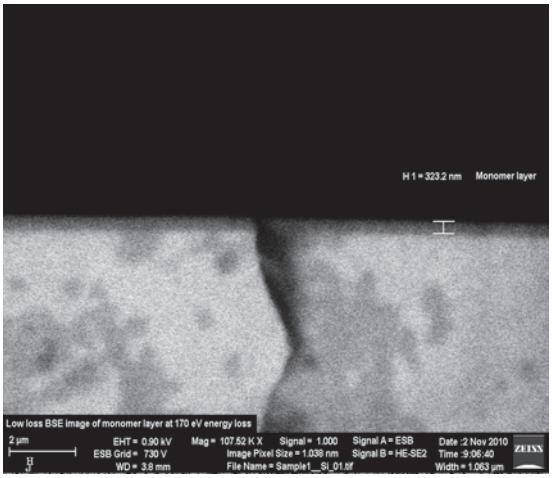

Fig. 7. Low Loss BSE imaging of cross section of PPHMDS layer.

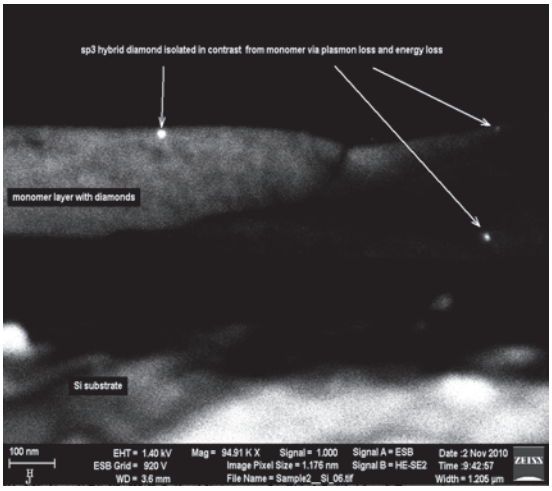

Fig. 8. Low loss BSE imaging of cross section of 6-DND/PPHMDS layer.

In Fig. 7, the image of PPHMDS grown on Si cross section is presented. The contrast, between Si substrate and the polymer layer with a thickness of 323.2 nm, is clearly displayed. On the base of the QCM (section 2.1.) and SEM measurements, the density of PPHMD layer was calculated to be in a range of 1.66 – 1.68 g/cm^3. In the next Fig. 8, the image of 6-DND/PPHMD grown on Si is presented. The sp^3 carbons appear as sphere-like bright spots with different size (5-20 nm). The layer thickness is 240 nm and the density is calculated to be 2.05 g/cm^3. The images of Si-DND/PPHMDS are presented in Fig. 9-a, and -b. As it is seen, Si-DND particles with sphere-like morphology of about 200 nm in size as well as very well defined triangle particle with (111) orientation are distinguished that corresponded to the HRTEM results (section 3.2.1.).

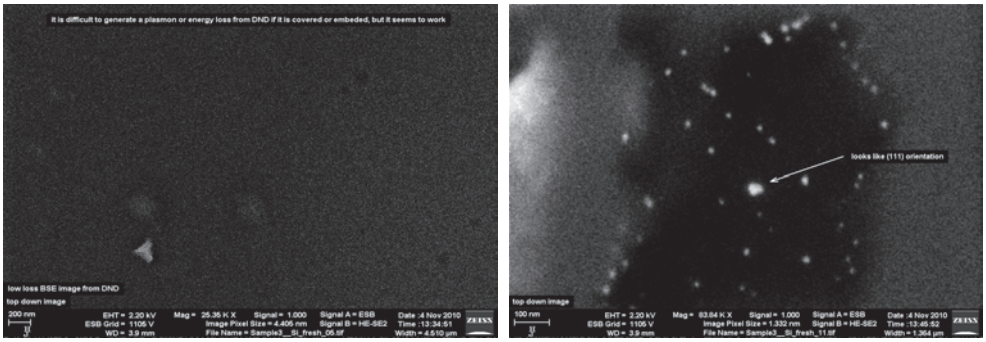

(a) (b)

Fig. 9. Low loss BSE imaging from DND particles, embeded inside the Si-DND/PPHMDS layer (a); Low loss BSE imaging of the Si-DND/PPHMDS surface (b).

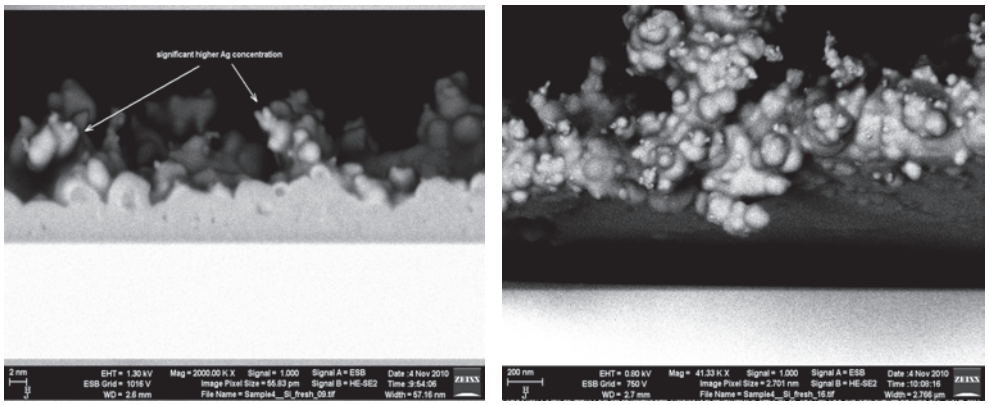

(a) (b)

Fig. 10. Low loss BSE imaging of the cross section of Ag-DND/PPHMDS (a) view in side (b).

The Ag-DND/PPHMDS image grown on Si is presented in Fig. 10-a, -b. Two parts of the layer are distinguished: the low part is dense with a thickness of about 125 nm, while the upper part is with significant concentration of Ag ions, with low density (about 0.4 g/cm^3) and a thickness of about 300 nm.

3.3.2 AFM of PPHMDS and DNDs/PPHMDS composites

The 3-D images and the roughness histogram (RH) of PPHMDS and Ag-DND/PPHMDS layers are shown in the Fig. 11-13. It is seen that Ag-DND/PPHMDS surface is rougher than the surface of PPHMDS and 6-DND/PPHMDS (see also Table 2 in section 3.3.3.). When treated for 5 min by NH_3 plasma, the RMS roughness extremely decreased up to 2.02 nm (Fig.13-b). This result is in agreement with the calculated density for the upper Ag-DND/PPHMDS/NH_3 layer from the SEM investigation.

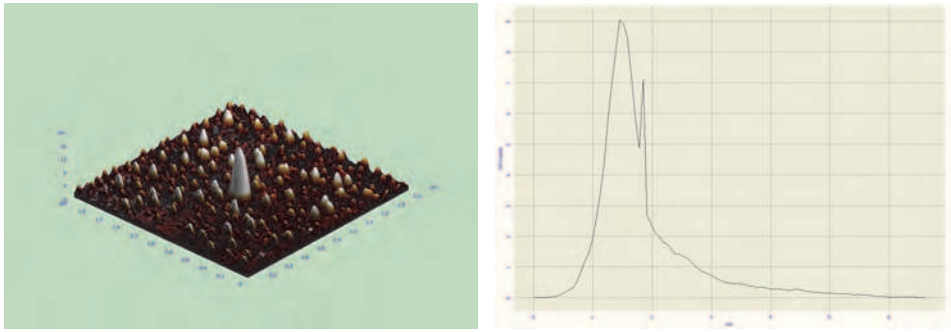

(a) (b)

Fig. 11. AFM 3-D image of PPHMDS on Si substrate; the image space is (x,y,z) = (2μm x 2μm x 16nm). (a); roughness histogram of 2D surface with image space (2μm x 2μm) (b);

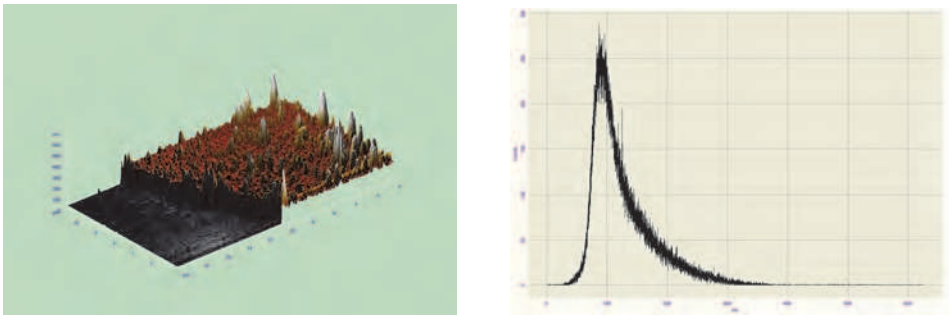

(a) (b)

Fig. 12. AFM 3-D image step of Ag-DND/PPHMDS and Si substrate; the image space is (x,y,z) = (10μm x 20μm x 600nm (a); roughness histogram of 2D surface with image space (20 μm x20 μm) (b);

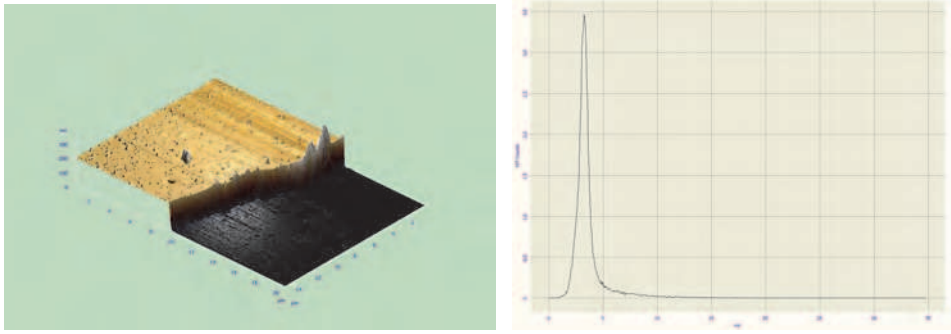

(a) (b)

Fig. 13. AFM 3-D image step of Ag-DND/PPHMDS/NH_3 and Si substrate; the image space is (x,y,z) = (20μm x 16μm x 300nm (a); roughness histogram of 2D surface with image space (20 μm x20 μm) (b);

Both AFM and SEM experiments disclose composite layers different topography which is related to the type of the used as filler DND and the particles peculiarity: spherical DND crystallites with sizes of few nanometers in the 6-DND/PPHMDS layer; specific Si-DND crystals with sizes up to few hundred nanometers immersed in the Si-DND/PPHNDS layer; spherical Ag-DND particles in the Ag-DND/PPHMDS layer. These differences result in a comparatively smooth 6-DND/PPHMDS surface and a rough surface for Si-DND/PPHMDS and especially for Ag-DND/PPHMDS (Table 2 in section 3.3.3.).

3.3.3 Contact angle of DNDs/PPHMDS and treated by NH_3

The CA of the different composites, and the corresponding treated by NH_3 plasma samples are presented in the Table 2. The CA of PPHMDS ($90^0 \pm 2^0$) is slightly increased for 6-DND/PPHMDS composite ($91^0 \pm 2^0$) and significant raised for 7-DND/PPHMDS(2) composite ($107^0 \pm 2^0$). The effect is due to the peculiarities of the used DNDs and the suspension type. The used alcohol 7-DND suspension is with increased amount of oxygenated residues on nanoparticles surface (Kurosawa, 2006 as cited in Pramatarova, 2010). The measured low CA value for Ag-DND/PPHMDS is due to the hydrophilic surface of Ag-DND sample. It is worth to note that the treated by NH_3 plasma Ag-DND/PPHMDS has similar CA ($75^0 \pm 2^0$). For all other composites the CA is diminished after 5 min ammonia treatment. The RMS roughness of all composites, with the exception of Ag-DND/PPHMDS, is equal. For Ag-DND/PPHMDS, the RMS roughness is extremely reduced from 50 nm to 2 nm after the ammonia treatment. The latter contradicts with the assumption that the roughness of the surface increase when the contact angle is reduced (www.ism.kiev.ua).

Sample - name	CA, [^{0}]	RMS roughness, [nm]	CA, after NH_3 treatment, [^{0}]
PPHMDS	90± 2	1.47	85± 2
6-DND/PPHMDS	91 ± 2	1,22	89± 2
7-DND/PPHMDS(2)	107± 2	1,23	60± 2
Ag-DND/PPHMDS	75 ± 2	50.38	75± 2

Table 2. Water contact angle (CA) and Root Mean Square (RMS) roughness of PPHMDS and DNDs/PPHMDS composites grown on CG.

The presented results confirm the influence of DNDs fillers and the ammonia plasma treatment on PPHMDS surface properties and on the CA change.

3.3.4 FTIR of DNDs/PPHMDS and treated by NH_3 plasma composites

The achieved surface modification of PPHMDS by DNDs filler could be followed by the characteristic band in the FTIR spectra (Fig 14). As seen from the FTIR spectra, a change of polymer characteristic bands is observed that is explained by penetration of DND particles in the polymer matrix. Well seen are the characteristic peaks for sp^3 bonded carbon at 1550 cm^{-1} and sp^2 bonded carbon at 1160 cm^{-1} of the DND. So, the surface of DNDs/PPHMDS is characterized with functional groups of the type –OH, >C=O, Si–O–Si, Si–O–C (Fig 14-2). The formation of new (C-Si-C) bonds and different tetrahedral CH_3 (the intensive bands in the region 2800 – 3000 cm-1) proved the existence of both hydrophobic and hydrophilic centers on DNDs/PPHMDS surfaces. In the case of Si-DND/PPHMDS (Fig 14-3), definite

peaks at around 500, 1200-1300, 1470 and 1600 cm^{-1} point for an increased content of amorphous carbon due to the silanization of DND particles. The appearance of intensive peak at 550 cm^{-1} in the spectrum of Ag-DND/PPHMDS (Fig 14-4) , the splitting of the peak at 1550 cm^{-1} into two peaks and the appearance of a broad band at 1800 cm^{-1} confirmed the location of Ag ions at the grain boundaries of diamond nanoparticles (Pramatarova et al., 20100.

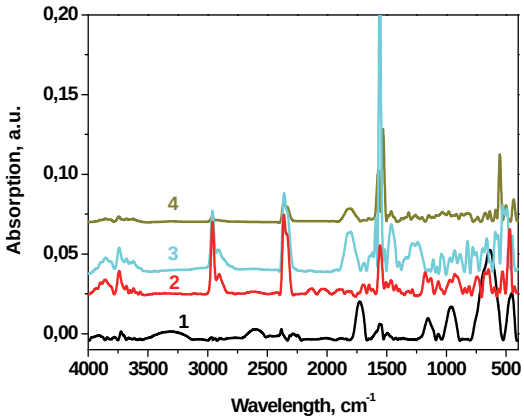

Fig. 14. FTIR spectra of (1) PPHMDS; (2) 6-DND/PPHMDS; (3) Si-ND/PPHMDS; (4) Ag-DND/PPHMDS;

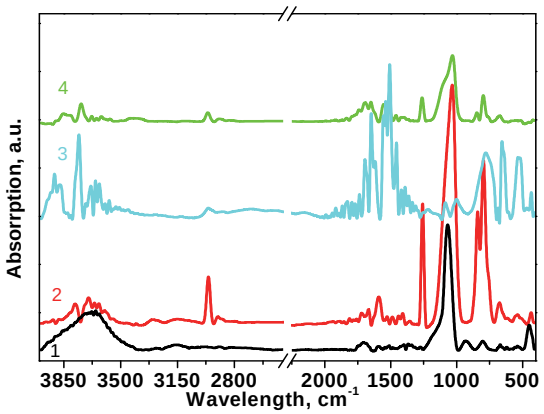

Fig. 15. FTIR spectra of (1) PPHMDS/NH_3; (2) 6-DND/PPHMDS/NH_3; (3) Si-DND/PPHMDS/NH_3; (4) Ag-DND/PPHMDS/NH_3;

The comparison of the spectra of the corresponding NH_3 plasma treated composites (Fig. 15) revealed that the surface functional groups of the composites are significantly modified. This is proved by the decrease in intensity of the bands for methyl groups, broadening and intensification of the bands in the region 3000 -3440 cm^{-1}, diminishing of the corresponding

1630 cm^{-1} and the bands in the region of surface functional groups. We affirm that the composite surface is with increased hydrophilic properties.

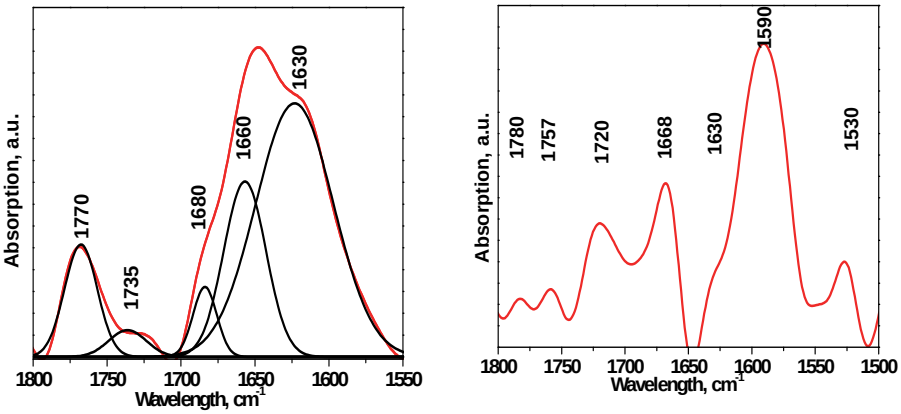

(a) (b)

Fig. 16. FTIR Deconvolution spectra in the range 1800 – 1500 cm^{-1} for the 6-DND_PPHMDS (a) and 6-DND_PPHMDS /NH_3 (b).

An overlay of the calculated contour of FTIR spectrum in the region of surface functional groups of 6-DND/PPHMDS and the corresponding spectrum after NH_3 treatment as determined by a curve fitting analysis is shown in Fig. 16. The comparison of the corresponding composites spectra proved the significant modification the surface functional groups.

3.3.5 Raman of DNDs/PPHMDS composites

For detailed analysis of characteristic bands, associated with bonding between the DNDs and PPHMDS, Raman microspectroscopy is used. In the Figure 17-a, b, c Raman spectra of DNDs/PPHMDS composites are presented. The assignment of characteristic vibrational bands is based on a comparison with the results in (Borjanovic et al., 2009, Pihan et al., 2009). The repeating unit of PPHMDS is –(Si(CH_3)$_2$-O)- with an Si-O-Si backbone and methyl side group attached to Si atoms. The Raman shift related to CH_3 vibration bands are as follows: 2967 and 2906 cm^{-1} (stretching) (Fig 17-c), 1413 and 1260 cm^{-1} (deformation) (Fig 17-b) and 865,756, and 688 cm^{-1} (rocking) (Fig 17-a). Raman spectra related to the C-Si-C groups are 845 and 790 cm^{-1} (asymmetric stretching) and 706 cm^{-1} (symmetric stretching). All characteristic Raman vibration bands of PPHMDS are also present in DNDs/PPHMDS composites. A new relatively intensive band at 1450 cm^{-1} is observed in all composites containing DND (Fig.17 b), To appreciate the possibilities of DNDs to modified the structure and the nature of chemical bonding of the polymer matrix (PPHMDS) further analysis of relative intensities of normal modes was performed following procedure described in (Borjanovic et al., 2009). The ratio of relative intensities I_{2967}/I_{2905} of CH_3 was lower in the composites (DNDs/PPHMDS) in comparison with PPHMDS. It was pronounced in the composites containing DND particles without any modification (6-DND and 7-DND). Such a tendency of decrease was also present in the vibrations of side chains (C-Si-C). The

observed changes in Raman and FTIR spectra (presented in 3.4.2.) of DNDs/PPHMDS verify the expected bonding between PPHMDS and DNDs nanoparticles.

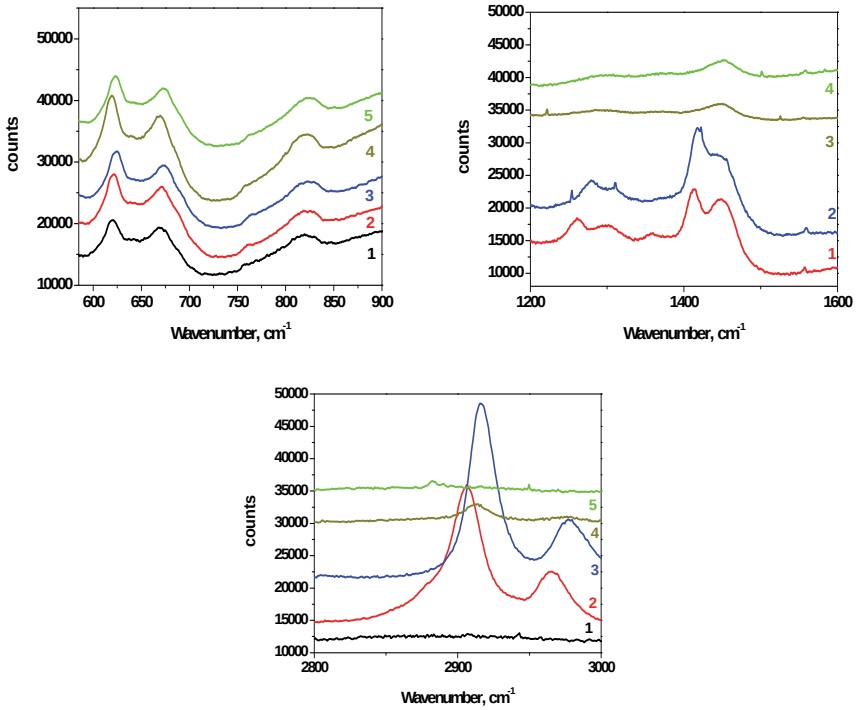

Fig. 17. (a) Raman spectra (600 – 900 cm^{-1}) (1) PPHMDS; (2) 6-DND/PPHMDS; (3) 7-DND/PPHMDS(2); (4) Ag-DND/PPHMDS; (5) Ag-DND/PPHMDS/NH_3;
(b) Raman spectra (1000 – 2000 cm^{-1}) (1) 6-DND/PPHMDS; (2) 7-DND_PPHMDS(2); (3) Ag-DND/PPHMDS; (4) Ag-DND/PPHMDS/NH_3;
(c) Raman spectra (2700– 3200 cm^{-1}) (1) PPHMDS; (2) 6-DND/PPHMDS; (3) 7-DND/PPHMDS(2); (4) Ag-DND/PPHMDS; (5) Ag-DND/PPHMDS/NH_3;

3.3.6 XPS of PPHMDS and DNDs/PPHMDS composites

The effect of the DNDs fillers on PPHMDS properties is studied by XPS technique. The XPS core level of C1s, O1s, Si2p, N1s, Ag3d as well as the Auger C KLL peaks are registered (Fig, 18 a, b). The samples surface composition is determined by the area of the corresponding components peaks, corrected with the photo-ionisation cross sections (Table 3).

No according XPS	Nomenclature	C [at%]	O [at%]	Si [at%]	N [at%]	Ag [at%]
1	6-DND/PPHMDS	45.8	22.9	29.5	1.8	-
3	Si-DND/PPHMDS	53.1	15.5	31.4	-	-
5	Ag-DND/PPHMDS	23.9	45.8	29.3	1.0	-
9	PPHMDS	6.8	54.9	38.2	-	-

Table 3. PPHMDS and DNDs/PPHMDS surface composition.

As seen from the table, the Ag3d peaks for Ag-DND/PPHMDS composites are not registered even after 10 min sputtering with 3 keV Ar + ions, which is probably due to the deep encapsulation of Ag ions. The peaks Si2p and O1s are recorded for all samples with energies at 103.5 and 533.2 eV, respectively, which are similar to the characteristic SiO_2 values. In Figure 1, the C1s spectra of the different samples were presented

The PPHMDS *C1s* peak (N9) is characterized by an energy of 284.6 eV, which is in accordance with the value published in the literature (Radeva et al., 1997). For the DNDs/PPHMDS composites, significant displacement of the binding energy of C1s peak to 285.7 eV is found Figure 18-a. These values are comparable with the values in the literature for sp^3 carbon energy in nanodiamonds (about 286.0 eV) (Merel et al., 1998). The high calculated semi-width of 2.3 eV, it could be suggested an existence of sp^3 carbon bounded to the polymer surface. The composite Si-DND/PPHMDS (N3) is characterized by a *C1s* peak at 285.8 and a semi-width of 1.7 eV that denoted an existence of sp^3 carbon on polymer surface. Ag-DND/PPHMDS composite (N5) is characterized by a broad peak with two similar maxima at about 286.0 and 284.6 eV that confirm an existence of carbon in different allotropic forms as sp^3 for the nanodiamond and sp^2 for the polymer. Important information, for the composites surface layers at about 1 nm depth, can be obtained from the analysis of C KLL Auger peak (Fig. 18-b). As it is seen, the PPHMDS's (N9) C KLL Auger peak is with a high kinetic energy of around 270.0 eV, a value characteristic for a C-Si bond. In the spectra of all composites two peaks are registered with maxima at about 265.0 and 272.0 eV., associated with sp^3 nanodiamond carbon (in the diamond it is at 262.2 eV) and carbon of the polymer chain. On the base of these two peaks correlation, an information for the composites surface is obtained.

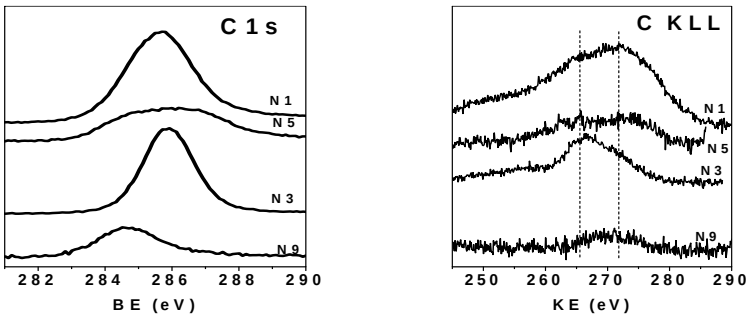

(a) (b)

Fig. 18. XPS core level C 1s (a) and C KLL Auger peak (b) of (N9) PPHMDS; (N1) 6-DND/PPHMDS; (N3) Si-DNS/PPHMDS; (N5) Ag-DND/PPHMDS;

The most intensive peak 272 eV is measured for 6-DND/PPHMDS composite (N1), which evidence for an increases nanodiamond concentration in polymer layer depth. The same was confirmed by the C1s peak. The measured value for Si-DND/PPHMDS composite (N 3) illustrates an enriched surface layer with nanodiamond particles.

The recorded peaks Si2p and O1s with energies at 103.5 and 533.2 eV, respectively, for all samples are similar to the characteristic SiO_2 values.

3.4 Biocompatibility studies

3.4.1 Cytotoxicity of DNDs

Recently it is reported that DND is less cytotoxic than other carbon materials (Schrand et al., 2009). However, the cytotoxicity of DND could be affected by its further chemical purification or modification. Hence, we have examined toxicity and biocompatibility of the DNDs used as fillers in PPHMDS. The results from this study are shown in Figure 19. As can be seen, the exposure of the cells to the supernatant (Fig.19, low panel) did not influence cell viability in a significant manner, suggesting an excellent biocompatibility. The osteoblasts formed nearly identical monolayers in all samples and we did not find any significant difference in the cell viability and the overall cell morphology after the incubation period of 3 days. When the cells were exposed to DNDs suspension, containing bigger nanoparticles and agglomerates (see sections 2.5.1. and 2.5.7) a slight reduction in the number of viable cells compared to supernatant (Fig.19, upper panel) was observed. Nevertheless, the attached cells were well spread suggesting unaffected cell functions. These results indicate that in the presence of DNDs the cells survive and grow well and thus confirm the literature data (Zhang et al., 2011).

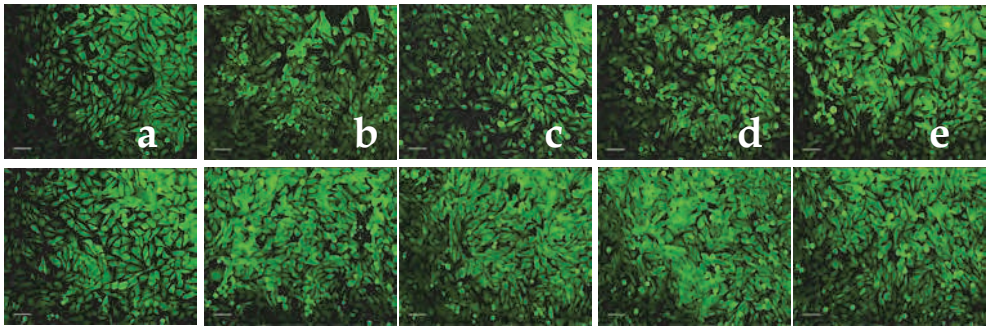

Fig. 19. Overall morphology of MG63 osteoblast incubated for 72 hours with suspension (upper panel) and supernatant (low panel), 6-DND (b); Si-DND (c);Ag-DND (d); 7-DND (e), respectively; culture medium+10% FCS was used as a control (a); bar, 100 µm.

3.4.2 Overall cell morphology on DNDs/PPHMDS

For a comprehensive characterization of the biocompatibility of the DNDs/PPHMDS coatings the initial interaction with osteoblast-like MG63 cells *in vitro* was studied. Osteoblasts are the principal cells in the bone matrix therefore their successful interaction with a material provides insights on its osseointegration. We examined the overall cell morphology, the organization of actin cytoskeleton and the focal adhesion complexes when cells adhering onto composite surfaces. In addition, we studied the effect of fibronectin (FN), which is the major adhesive protein in biological fluids and play significant role for the initial interaction of cells with biomaterials.

The change in the overall cell morphology and in the number of attached cells on composite is demonstrated in Fig. 20. When cells were cultured on plain (FN non-coated) surfaces they were small and round in shape (Fig.20, upper panel) and no significant organization of actin was detected (data not shown). As expected, FN pre-coating improved the cellular interaction to all surface. On non-coated surfaces, the number of attached cells was highest

on Si-DND/PPHMDS (Fig. 20-c, upper panel), whereas within FN pre-coated surfaces cells adhered more readily on Ag-DND/PPHMDS (Fig. 20-d, low panel). Interestingly, on FN-coated 6-DND/PPHMDS layers (Fig.20-b, lower panel), the cells represented varying morphology suggesting different stages of adhesion. On Si-DND/PPHMDS and especially on Ag-DMD/PPHMDS the osteoblast were well spread and exhibited an organized cytoskeleton with well expressed actin fibers (Fig. 20, low panel and Fig. 21 c, d, upper panel). Further, we study the distribution of vinculin as a prominent component of focal adhesions (Zamir et al., 2001, Geiger et al., 2001) that links the cytoskeleton, plasma membrane, and ECM (Katz et al., 2000).

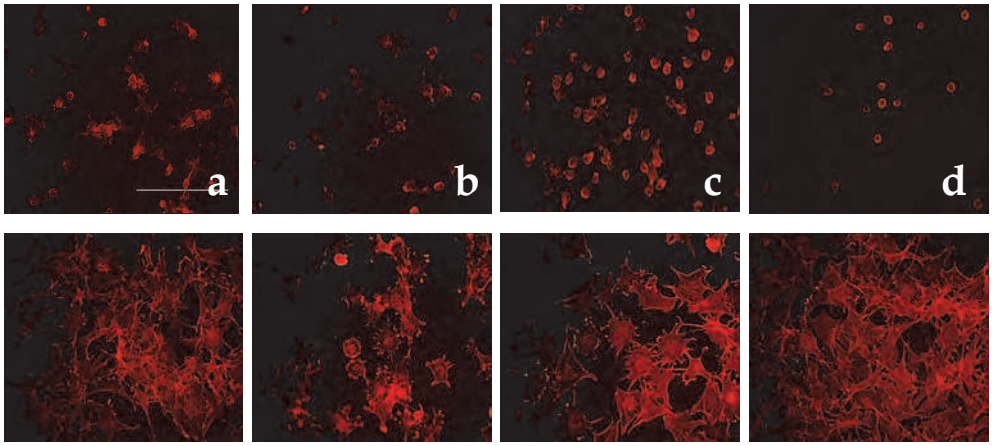

Fig. 20. Overall morphology of MG63, cultured for 2 hours on control glass coverslips (a); 6-DND/PPHMDS (b); Si-DND/PPHMDS (c) and Ag-DND/ PPHMDS (d). Materials were studied as plain (upper panel), or pre-coated with FN (low panel); bar 100μm.

As shown in Fig. 21, low panel, on Si-DND/PPHMDS and Ag-DND/PPHMDS composites vinculin was arranged in streaks at cell periphery, similarly to control. In contrast, on 6-DND/PPHMDS vinculin was limited to the edge of osteoblast lamellipodia and rather diffuse distribution throughout the cell body (Fig. 21-b low panel).
The improved cell morphology, cytoskeleton organization and focal adhesion formation on Si-DND/PPHMDS and Ag-DND/PPHMDS composites was believed to be a result of the composites surface properties that depend on DNDs filler. However, not only the chemistry, but the wettability and nanotopography are the factors that are changed in these composites. As we showed in section 3.3.3, introducing Ag-cations into composite material resulted in an increased surface hydrophilicity as well as surface roughness. Many papers demonstrated that hydrophilic surfaces support cellular interaction in comparison to hydrophobic ones (Grinnell, Feld, 1982, Altankov et al., 1996, 1997), which is in accordance to our results. It is known however (Barrias et al., 2009) that the surface properties of biomaterials influence cell behaviour through the adsorbed serum proteins and proteins secreted by cells themselves. It is not only the adsorbed quantity, but also the protein conformation will determine the cellular interaction. Therefore, in our future experiments we plan to study in details FN conformation upon adsorption of DNDs/PPHMDS composite layers.

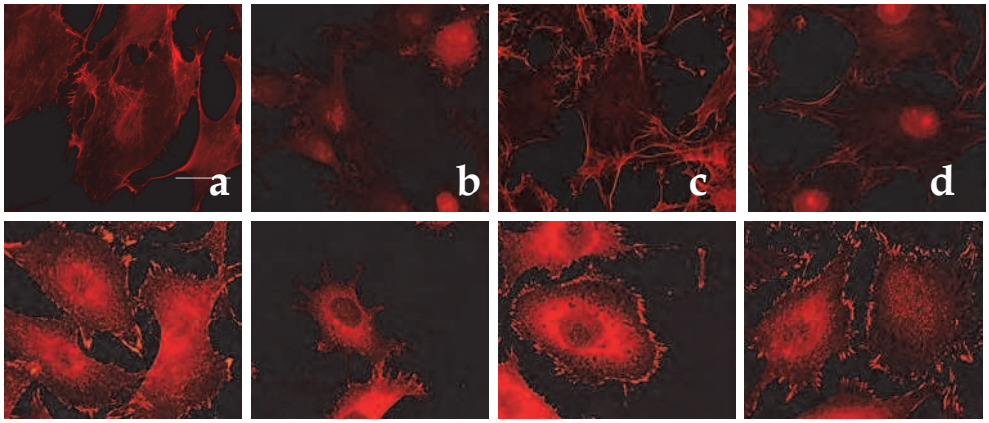

Fig. 21. Actin (upper panel) and Vinculin (low panel) staining of MG63, cultured for 2 hours on FN coated plain glass coverslips, used as a control (a), 6-DND/PPHMDS (b); Si-DND/PPHMDS (c) and Ag-DND/PPHMDS (d); bar 50μm

3.4.3 Biocompatibility study of DNDs/PPHMDS treated by NH_3 plasma

We further studied the effect of NH_3 plasma treatment of Si-DND/PPHMDS and Ag-DND/PPHMDS on the initial osteoblast adhesion (Fig. 22 and 23). We used NH_3 plasma , because it has been demonstrated [Chen et al., 2003, Yang et al., 2002, Krasteva et al., 2010] that such treatment is an easy way to render a hydrophobic surface into hydrophilic and thus to derive substrates that support the attachment and growth of anchorage dependent cells. Here, we studied the overall cell morphology and the development of the specific adhesive structures - focal adhesion contacts.

We observed a poor spontaneous osteoblast adhesion on all non-coated samples, treated by NH_3 plasma (Fig.22, upper panel), similar to those without any plasma treatment (Fig.20, upper panel). Again, more cells were detected on Si-DND/PPHMDS/NH_3 as on glass control, compared to Ag-DND/PPHMDS/NH_3. Following FN pre-adsorption, the number of attached and spread cells (Fig. 22, low panel) as well as the organization of actin cytoskeleton and focal adhesion contacts as can be seen on the next figure (Fig. 23) improved dramatically. In general, NH_3 plasma treated composite layers seems to promoted osteoblast adhesion making it indistinguishable from the "golden control" – glass surface. The biological effect of NH_3 plasma treatment presumably is associated with the generation of hydrophilicity. However, our studies did not revealed direct correlation between the increased hydrophilicity and the observed biological effects. Ammonia plasma introduces polar amine functional groups onto PPHMDS films, as evidenced above by FTIR records (Fig. 2. section 3.1.1.) and thus changes both surface chemistry and surface hidrophilicity. Many studies reported increased FN adsorption on NH_2-functionalized surfaces (Gustavsson et al., 2008). Thus, the increased osteoblast affinity to FN pre-coated NH_3 plasma treated layers could be explained also by increased binding of FN. The observed high spontaneous cell adhesion but not cell spreading on non-coated, Si-DND/PPHMDS treated by NH_3 samples was probably due to a combination of increased adsorption of newly synthesized adhesive proteins by the cells and from the fact that the cells could easily overcome the electrostatic barrier-effect that could promote both faster adhesion and cell spreading.

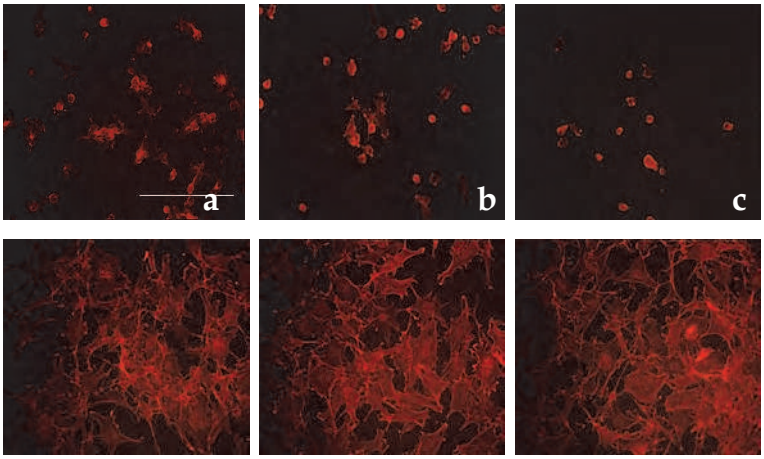

Fig. 22. Overall morphology of MG63, cultured for 2 hours on control glass coverslips (a); Si-DND/PPHMDS/NH3 (b) and Ag-DND/PPHMDS/NH3 (c) viewed by actin staining; Materials were studied as plain (upper panel), or pre-coated with FN (low panel); bar 100μm.

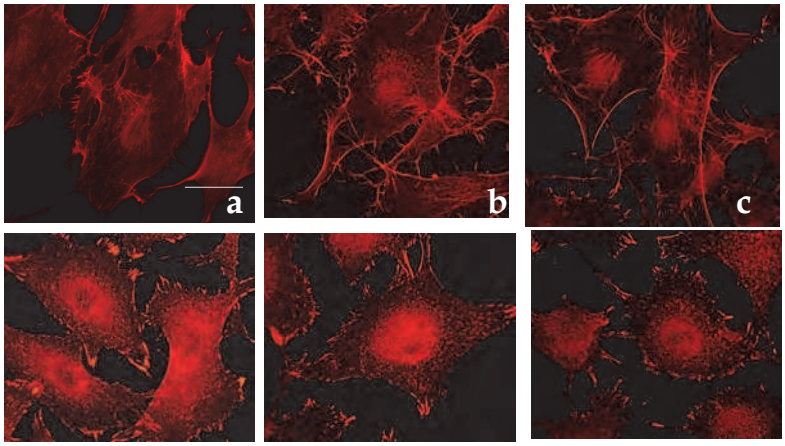

Fig. 23. Actin (upper panel) and Vinculin (lower panel) staining of MG63, cultured for 2 hours on FN coated plain glass control glass coverslips (a), Si-DND/PPHMDS/NH3 (b) and Ag-DND/PPHMDS/NH3 (c); bar 50μm.

4. Conclusions

The plasma polymerization of the well know hexamethyldisiloxane monomer is used for deposition of PPHMDS layers with excellent adhesion on different substrates and remarkable properties. For the first time, composites of the type DNDs/PPHMDS are obtained and precisely characterized by different physicochemical methods.
The most important result of the study is that by varying DNDs particles type, it is possible to alter the morphological and chemical nature, as well as the biological performance of the

resultant composite layers. The treatment of composites surface by ammonia plasma reduce its surface hydrophobisity.
The cytotoxicity test indicates that the cells survive and also grow well in presence of DNDs. The biological studies performed under short term cultures of osteoblast-like MG63 cells proved that on the plain surface of Si-DND/PPHMDS composite, the number of the attached cells is the highest. FN pre-coating improved the celular interaction to all surface, but the cell adhered more readily on Ag-DND/PPHMDS. The same effect is observed after treatment by ammonia plasma.

5. Acknowledgments

This research was financially supported by the Bulgarian National Science Foundation (Grant TK-X 1708/07), Bulgarian National Innovation Foundation (Grant 02-54/07). The authors would like to thank Prof. G. P. Bogatyreva for providing DND suspension. The authors thank Dr. J. Heiner, Dr. Ph. Kern and Dr. J. Werckmann for their support with the SEM, AFM and TEM measurements, respectively. The financial support of Spanish Ministry for Research and Education: grant MAT2009-14440-C02-02 (to GA) is also acknowledged, as well as, the ANNA project (№ 026134(RI3) provided to IBF from the FP6 Research Infrastructure Action "European Integrated Activity of Excellence and Networking for Nano and Micro-Electronics Analysis".

6. References

Agarwal A, Weis T L, Schurr M j, Faith N G, Czuprynski C J, McAnulty J F, Murphy Ch J & Abbott N L. (2009). Surfaces modified with nanometer-thick silver-impregnated polymeric films that kill bacteria but support growth of mammalian cells. *Biomatieials*. dio: 10.1016/j.biomaterials.2009.09092

Altankov G, Grinnell F & Groth T .(1996). Studies on the biocompatibility of materials: fibroblast reorganization of substratum-bound fibronectin on surfaces varying in wettability. *J Biomed Mater Res* 30: 385-391.

Altankov G, Groth T, Krasteva N, Albrecht W & Paul D. (1997). Morphological evidence for a different fibronectin receptor organization and function during fibroblast adhesion on hydrophilic and hydrophobic glass substrata. *J Biomater Sci Polymer* Ed 8: 721-740.

Baidakova M & Vul' A . (2007). New prospects and frontiers of nanodiamond clusters. *J. Phys. D: Appl. Phys.* 40 6300-6311

Barrias C C, Martins M C L, Almeida-Porada G, Barbosa M A & Granja P L. (2009). The correlation between the adsorption of adhesive proteins and cell behaviour on hydroxyl-methyl mixed self-assembled monolayers. *Biomaterials*, 30.; 307-316.

Bogatyreva G P, Voloshin M N & Padalko V I. (2008). Detonation synthesized nanodiamond powder for the preparation of porous polycrystalline micron powders. *Diamond & Related Materials. 17*, 213–216 ISSN: 0925-9635

Borjanovic V, Bistricic L, Vlasov I, Furic K, Zamboni I, Jaksic M & Shenderova O. (2009). Influence of proton irradiation on the structure and stability of poly(dimethylsiloxane) and poly(dimethylsiloxane)-nanodiamond composite. *J. Vac. Sci. Technol*. B.; 27; 6; 2396-2430

Borjanovic V, Lawrence W G, Hens Suzanne, Jaksic M, Zamboni I, Edson C, Vlasov I, Shenderova O & McGuire G E. (2009). Effect of proton irradiation on photoluminescent properties of PDMS-nanodiamond composites. *Nanotechnology*. 19; 1-10

Chen M, Zamora P O, Som P, Pena L A & Osaki S. (2003). Cell attachment and biocompatibility of polytetrafuoroethylene (PTFE) treated with glow-discharge plasma of mixed ammonia and oxygen. *J. Biomater. Sci. Polymer Edn*. 14.; 9.; 917–935

Dolmatov V Yu .(2007). Composite materials based on elastomer and polymer matrix, filled with detonation nanodiamonds. *Russian Chemical Reviews.* 70.; 7.; 607-626

Geiger B, Bershadsky A, Pankov R & Yamada K M. (2001). Transmembrane crosstalkbetween the extracellular matrix—cytoskeleton crosstalk. *Nat Rev Mol Cell Biol*. 2(11).; 793–805.

Grinnell F & Feld M K .(1982). Fibronectin adsorption on hydrophilic and hydrophobic surfaces detected by antibody binding and analyzed during cell adhesion in serumcontaining medium. *J Biol Chem.* 257.; 4888-4893.

Gustavsson J, Altankov G, Errachid A, Samitier J, Planell JA & Engel E. (2008). Surface modifications of silicon nitride for cellular biosensor applications. *J Mater Sci Mater Med.* 19.; 4.; 1839-1850.

Heiner J (2008). Low Loss BSE Imaging with ZEISS ULTRA GEMINI® technology. *In www.smt.zeiss.com/NTS*

Heuer A H et al .(1992). Inovative materials processing strategies: a biomimetic approach. *Science.* 255.; 5048.; 1098 – 1105.

Hong C-S, Park H H, Wang S J, Moon J, Park H H & Hill R H. (2006). Formation of photoresist-free patterned ZnO film containing nano-sized Ag by photochemical solution deposition. *Applied Surface Science.* 252.; 21., 7739–7742

Krasteva N, Toromanov G, Hristova K T, Radeva E I, Pecheva E V, Dimitrova R P, Altankov G P & Pramatarova L D. (2010). Initial biocompatibility of plasma polymerized hexamethyldisiloxane films with different wettability. *Journal of Physics: Conference Series 253*.; 012079 doi:10.1088/1742-6596/253/1/012079

Katz B Z, Zamir E, Bershadsky A, Kam Z, Yamada K M & Geiger B. (2000). Physical state of the extracellular matrix regulates the structure and molecular composition of cell–matrix adhesions. *Mol Biol Cell*. 11.; 3.; 1047–1060.

Krasteva N, Hristova K, Radeva E, Pecheva E, Dimitrova R & Pramatarova L. (2010). Effect of ammonia plasma treatment on the biological performance of plasma deposited polyhexadimethylsiloxane. *CP1203 American Institute of Physics*. 688-693

Lowenstam H A & Weiner S. (1989). *On biomineralization*. Ed. New York.; Oxford Press

Merel P, Tabbal M, Chaker M, Moisa S & Margot J. (1998). Direct evaluation of sp^3 content in diamond-like-carbon films by XPS. *Appl. Surf. Sci.;* 136.; 105-109.

Min-Hsien. (2009). Simple poly(dimethylsiloxane) surface modification to control cell adhesion. *Surf. Interface Anal.;* 41.; 11–16

Mitev D, Dimitrova R, Spassova M, Minchev Ch & Stavrev S. (2007) Surface Peculiarities of Detonation Nanodiamonds in Dependence of Fabrication and Purification Methods. *Diamond and Related Materials*. 16.; 4-7.; 776-780

Murphy J & Jana N R. (2002). Controlling the aspect ratio of inorganic nanorods and nanowires. *Advanced Materials*. 14.;1.; 80–82

Nobbmann U & Morfesis A. (2009). Light scattering and nanoparticles. Materialstoday. 12; 5.; 52-54

Pihan S A, Tsukruk T & Forch R. (2009). Plazma polymerized hexamethyl disiloxan in adhesion applications. *Surface and Coatings Technology*. 203.;13; 1856-1862

Pramatarova L, Pecheva E, Stavrev S, Spasov T, Montgomery P, Toth A, Dimitrova M & Apostolova M. (2007). Artificial bones through nanodiamonds. *Journal of Optoelectronics and Advanced Materials*. 9.; 1.; 236-239

Pramatarova L D, Krasteva N A, Radeva E I, Pecheva E V, Dimitrova R P, Hikov T A, Mitev D P, Hristova K T & Altankov G. (2010). Study of detonation nanodiamond – plasma polymerized hexamethildisiloxan composites for medical application. *J. Phys.: Conf. Ser. 253*; 012078

Radeva E, Tsankov D, Bobev K & Spassov L. (1993). Fourier transform infrared analysis of hexamethyldisiloxane layers obtained in low-frequency glow discharge. *J. Appl. Polym. Sci*. 50.; 165-169

Radeva E, Tsankov D, Bobev K & Spassov L. (1993). Fourier Transform Infrared Analysis of Hexamethyldisiloxane Layers Obtained in Low-frequency Glow Discharge. *J. Appl. Polym. Sci*. 50.; 165-171

Radeva E, Stefanov P & Spasov L. (1997). X-ray photoelectron spectroscopy study on chemical structure of plasma-polymerized hexamethyldisiloxan. *Comptes rendus de lÁcademie Bulgare des Aciences*. 50.; 9-10.; 19-22

Radeva E & Spassov L. (1998). Effect of plasma polymerization conditions on the humidity sorptive properties of thin films obtained from hexamethyldisiloxane in glow discharge. *Vacuum*. 55.; 217-220

Radeva E, Pramatarova L, Pecheva E, Hikov T, Iacob E, Vanzetti L, Dimitrova R, Krasteva N, Spassov T & Fingarova D. (2010). Study of organosilicon plasma polymer used in composite layers with biomedical application. *CP1203 American Institute of Physics*. 949-954

Salmerón-Sánchez M & Altankov G. (2010). Cell-Protein-Material interaction in tissue engineering. *Tissue Engineering*. Ed. by Daniel Eberli MD. PhD. Published by In-Teh. 077-103

Schrand A M, Johnson J, Dai L M, Hussain M, Schlager J J & Zhu L. (2009). Cytotoxicity and genotoxicity of carbon nanomaterials. *In: Webster TJ, editor. Safety of nanoparticles. From manufacturing to medical applications. New York: Springer;*. 159-187.

Shenderova O A, Zhirnov V V & Brenner D W. (2002). Carbon nanostructures. *Solid State Mater.Sci*. 27; (3/4).; 227-356

Stavrev S, Lazarov S, Stoev Kh, Markov L & Ivanov V. (1994). *US patent* No 5353708

Tsankov D, Radeva E, Hinrichs K, Rfseler A & Korte E.-H. (2005). Infrared spectroscopic ellipsometry and atomic force microscopy study of plasma polymerized hexamethyldisiloxane layers post-treated by NH3 plasma. *Thin Solid Films*. 476.; 174–180

Vasilev K, Sah V, Anselm K, Ndi C, Mateescu M, Dollmann B, Martinek P, Ys, Ploux L & Griesser H J. (2010). Tunable Antibacterial Coatings That Support Mammalian Cell growth. *Nano Letter*. 10.; 202-207

Yang J, Shi G, Bei J, Wang S, Cao Y, Shang Q,Yang G & Wang W. (2002). Fabrication and surface modification of macroporous poly(L-lactic acid) and poly(L-lactic-*co*-glycolic acid) (70/30) cell scaffolds for human skin fibroblast cell culture. *J Biomed Mater Res*. 62.; 438–446

Zhang Q, Mochalin V N, Neitzel I, Knoke I, Han J, Klug C A, Zhou J G, Lelkes P I & Gogotsi Y. (2011). Fluorescent PLLA-nanodiamond composites for bone tissue engineering, *Biomaterials*. 32.; 87-94

Zhao B, Hu H, Mandal S K & Haddon R C A. (2005). Bone Mimic Based on the Self-Assembly of Hydroxyapatite on Chemically Functionalized Single-Walled Carbon Nanotubes. *Chem. Mater.*, 17(12).; 3235-3241.

Zamir E & Geiger B. (2001). Molecular complexity and dynamics of cell–matrix adhesions. *J Cell Sci.*;114(Pt 20).; 3583–3590. *www.ism.kiev.ua*

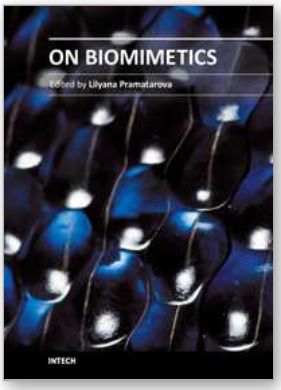

On Biomimetics

Edited by Dr. Lilyana Pramatarova

ISBN 978-953-307-271-5
Hard cover, 642 pages
Publisher InTech
Published online 29, August, 2011
Published in print edition August, 2011

Bio-mimicry is fundamental idea â€˜How to mimic the Natureâ€™ by various methodologies as well as new ideas or suggestions on the creation of novel materials and functions. This book comprises seven sections on various perspectives of bio-mimicry in our life; Section 1 gives an overview of modeling of biomimetic materials; Section 2 presents a processing and design of biomaterials; Section 3 presents various aspects of design and application of biomimetic polymers and composites are discussed; Section 4 presents a general characterization of biomaterials; Section 5 proposes new examples for biomimetic systems; Section 6 summarizes chapters, concerning cells behavior through mimicry; Section 7 presents various applications of biomimetic materials are presented. Aimed at physicists, chemists and biologists interested in biomineralization, biochemistry, kinetics, solution chemistry. This book is also relevant to engineers and doctors interested in research and construction of biomimetic systems.

How to reference

In order to correctly reference this scholarly work, feel free to copy and paste the following:

L. Pramatarova, E. Radeva, E. Pecheva, T. Hikov, N. Krasteva, R. Dimitrova, D. Mitev, P. Montgomery, R. Sammons and G. Altankov (2011). The Advantages of Polymer Composites with Detonation Nanodiamond Particles for Medical Applications, On Biomimetics, Dr. Lilyana Pramatarova (Ed.), ISBN: 978-953-307-271-5, InTech, Available from: http://www.intechopen.com/books/on-biomimetics/the-advantages-of-polymer-composites-with-detonation-nanodiamond-particles-for-medical-applications

INTECH
open science | open minds

InTech Europe
University Campus STeP Ri
Slavka Krautzeka 83/A
51000 Rijeka, Croatia
Phone: +385 (51) 770 447
Fax: +385 (51) 686 166
www.intechopen.com

InTech China
Unit 405, Office Block, Hotel Equatorial Shanghai
No.65, Yan An Road (West), Shanghai, 200040, China
中国上海市延安西路65号上海国际贵都大饭店办公楼405单元
Phone: +86-21-62489820
Fax: +86-21-62489821